Geochemical Perspectives Letters

Tin isotopic fractionation during igneous differentiation and Earth's mantle composition

N. Badullovich[1], F. Moynier[1,2*], J. Creech[1], F.-Z. Teng[3], P.A. Sossi[1]

OPEN ACCESS

doi: 10.7185/geochemlet.1741

Abstract

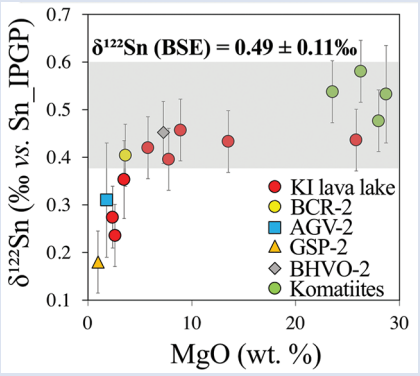

Tin exists both under the 2+ and 4+ oxidation states in igneous systems, and thus its geochemical behaviour changes as a function of oxygen fugacity. To characterise the redox state of Sn during magmatic differentiation and how this affects its isotope composition, we have measured Sn isotopic and elemental abundances in a suite of samples from the Kilauea Iki lava lake. Sn behaves as a highly incompatible element during fractional crystallisation. Lattice strain modelling shows that Sn^{2+} has mineral-melt partition coefficients ($D^{min/melt}$) ≈ 1 in plagioclase and clinopyroxene, whereas it is highly incompatible in all phases save for ilmenite, attesting to the sole presence of Sn^{4+} in basaltic liquid at the Fayalite-Magnetite-Quartz (FMQ) buffer. Furthermore, Sn isotopes are unfractionated during crystallisation of silicates, but decrease to lighter values upon ilmenite precipitation. Isotopic fractionation is onset by the coordination change between Sn^{4+} in the melt (6- to 8-fold) and ilmenite (6-fold). The Sn isotope composition of komatiites, which are high degree, high temperature partial melts are used to estimate the Sn isotope composition of the bulk silicate Earth (BSE). Komatiites have $\delta^{122}Sn$ within the range of the basalts (before ilmenite precipitation) and together provide the best estimate of the BSE of 0.49 ± 0.11 ‰ (2 s.d., n = 9).

Received 12 April 2017 | Accepted 28 September 2017 | Published 15 November 2017

Letter

Moderately volatile elements (MVEs) and their isotopes are important tracers for planetary and nebular processes such as evaporation and condensation (*e.g.*, O'Neill and Palme, 2008; Paniello *et al.*, 2012). A condition that must be met before MVEs can be used to answer these questions is knowledge of the isotopic composition of the bulk silicate Earth (BSE) and hence how their isotopes fractionate during igneous processes.

Tin has three oxidation states (Sn^0, Sn^{2+}, Sn^{4+}) that confer differing properties as a function of oxygen fugacity (fO_2). As such, Sn may behave as a siderophile, chalcophile and lithophile element at high temperatures (*e.g.*, Heinrich, 1990; Witt-Eickschen *et al.*, 2009). Although the dependence of Sn^{2+}/Sn^{4+} on melt composition, and the fO_2 at which this transition occurs in basaltic melts are poorly known (Farges *et al.*, 2006), the behaviour of Sn in igneous systems may be gleaned by comparison with elements of similar incompatibility. Observations of oceanic basalts show that Sn/Sm, Sn/Zr and Sn/Hf ratios are nearly uniform across MORB and OIB (Jochum *et al.*, 1993; Jenner and O'Neill, 2012). Correlations with tetravalent, incompatible elements suggest Sn may be lithophile and occurs as Sn^{4+} during igneous processes near FMQ.

At equilibrium, all else being equal, isotopic fractionation is controlled by differences in bond stiffness between two phases (*e.g.*, Schauble, 2004). The diversity in Sn bonding environments (Sn-O, Sn-S and Sn^0) combined with differing oxidation states offer scope for significant isotope fractionation. Indeed, Creech *et al.* (2017) analysed four genetically unrelated igneous rocks and identified that the $^{122}Sn/^{118}Sn$ ratio increases with increasing MgO content, suggesting that Sn isotopic fractionation occurs during igneous differentiation. However, the mechanisms driving this fractionation remain unknown.

In order to determine the behaviour of Sn isotopes in igneous systems and establish the composition of the BSE, it is necessary to investigate natural terrestrial samples from a common source. Kilauea Iki (KI) lava lake is well-suited to test the effects of fractional crystallisation (*e.g.*, Tomascak *et al.*, 1999; Teng *et al.*, 2008; Chen *et al.* 2013; Kato *et al.*, 2017). The cooling lava differentiated in a closed system to form olivine-rich cumulates to andesitic lavas with some rare silicic veins. Extrapolation to the composition of the BSE using a single magmatic suite is tenuous, given the diversity of mantle sources in the present day mantle and the possibility of secular changes in mantle composition (*e.g.*, Maier *et al.*, 2008). In order to assess mantle heterogeneity over space and time, komatiites, ranging in age from 3.5 to 2.7 Ga and from 3 cratons

1. Institut de Physique du Globe de Paris, Université Sorbonne Paris Cité, Université Paris Diderot, 1 rue Jussieu, 75238 Paris cedex 05, France
2. Institut Universitaire de France, 75005 Paris, France
* Corresponding author (email: moynier@ipgp.fr)
3. Department of Earth and Space Sciences, University of Washington, Seattle, USA

(Yilgarn, Kaapvaal, Superior), were analysed for their Sn isotope composition. As komatiites are produced by 25–40 % partial melting (*e.g.*, Herzberg, 1992), and Sn is incompatible during mantle melting (being predominantly hosted in clinopyroxene; Witt-Eickschen *et al.*, 2009), melting quantitatively extracts Sn from their mantle sources. Komatiite sources, especially for older 3.5 Ga examples, have primitive mantle-like compositions (Sossi *et al.*, 2016), and thus permit assessment of the temporal and chemical heterogeneity in Earth's mantle.

Here, we have analysed the isotopic composition of a series of samples from KI lava lake and komatiites utilising the ^{117}Sn-^{122}Sn double spike MC-ICPMS method described by Creech *et al.* (2017) (see Supplementary Information). The differentiation sequence samples form a sub-alkali series with MgO content ranging from 25.83–2.37 wt. % (Helz *et al.*, 1994) (see Supplementary Information). The four spinifex-textured komatiites have 23.54 < MgO (wt. %) < 28.71, and thus chemical compositions close to their respective parental magma (Sossi *et al.*, 2016).

The data are reported in Table 1, with δ^{122}Sn being the ‰ deviation of the ^{122}Sn/^{118}Sn ratio relative to the Sn_IPGP standard. In the KI samples, δ^{122}Sn ranges from 0.24 ± 0.07 to 0.46 ± 0.07 ‰, which represents a variation (~0.05 ‰/amu) similar to Zn (~0.05 ‰/amu; Chen *et al.*, 2013). The samples with less than 5 wt. % MgO show a progressive depletion in the heavier isotopes of Sn as MgO decreases (Fig. 1b). In addition, Sn concentration inversely correlates with the MgO content of the samples, defining a parabolic curve typical of highly incompatible elements (Fig. 1a). The Sn/E ratios (E = Sm, Hf or Zr; data from Helz, 2012) in samples across the differentiation sequence are similar to OIBs and MORBs reported in Jochum *et al.* (1993) and Jenner and O'Neill (2012) (see Supplementary Information). The four komatiites have different Sn contents between 0.15 and 0.36 ppm (BSE = 0.14 ppm), however, their δ^{122}Sn fall between 0.48 ± 0.065 ‰ and 0.58 ± 0.065 ‰, and show no systematic differences.

To understand the Sn isotopic variations, it is necessary first to estimate the partition coefficients of Sn^{2+} and Sn^{4+} between major minerals and melt. Given the limited experimental data currently available (Adam and Green, 2006; Klemme *et al.*, 2006; Michely *et al.*, 2017), we address this question using lattice strain theory and then model the Sn abundance and speciation during the differentiation of the KI lava lake.

Calculating elemental partitioning of Sn. Partition coefficients for Sn^{2+} and Sn^{4+} between crystals and melt were calculated for olivine, clinopyroxene, orthopyroxene, plagioclase and ilmenite using the lattice strain model (Blundy and Wood, 1994; Supplementary Information). The calculated values were then compared to experimentally derived partition coefficients (Michely *et al.*, 2017; Adam and Green, 2006; Klemme *et al.* 2006; Table 2). Stannous Sn^{2+} (r_{VI} = 0.96 Å) substitutes poorly into the M1 sites of Fe-Mg silicates ($D^{min/melt} \approx 0.1$), but has $D^{min/melt}$ of unity in the larger, Ca-bearing VIII-fold sites of clinopyroxene and plagioclase ($r_{VIII} \approx 1.15$ Å). Divalent tin is more compatible in all minerals except ilmenite compared to Sn^{4+} (r = 0.69 Å) due to its substitution for $^{VI}Ti^{4+}$ (r = 0.605 Å). The experiments of Michely *et al.* (2017), performed in air, contain exclusively Sn^{4+}, whereas those of Adam and Green (2006) may contain both Sn^{2+} and Sn^{4+} because Sn falls between calculated lattice strain curves for a given redox state and site property. The graphite capsules used imposed fO_2 conditions near FMQ-2 (Médard *et al.*, 2008), at least 2 orders of magnitude lower than in the KI lava lake, thereby increasing the stability of divalent Sn, according to:

$$SnO + \frac{1}{2}O_2 = SnO_2 \qquad \text{Eq. 1}$$

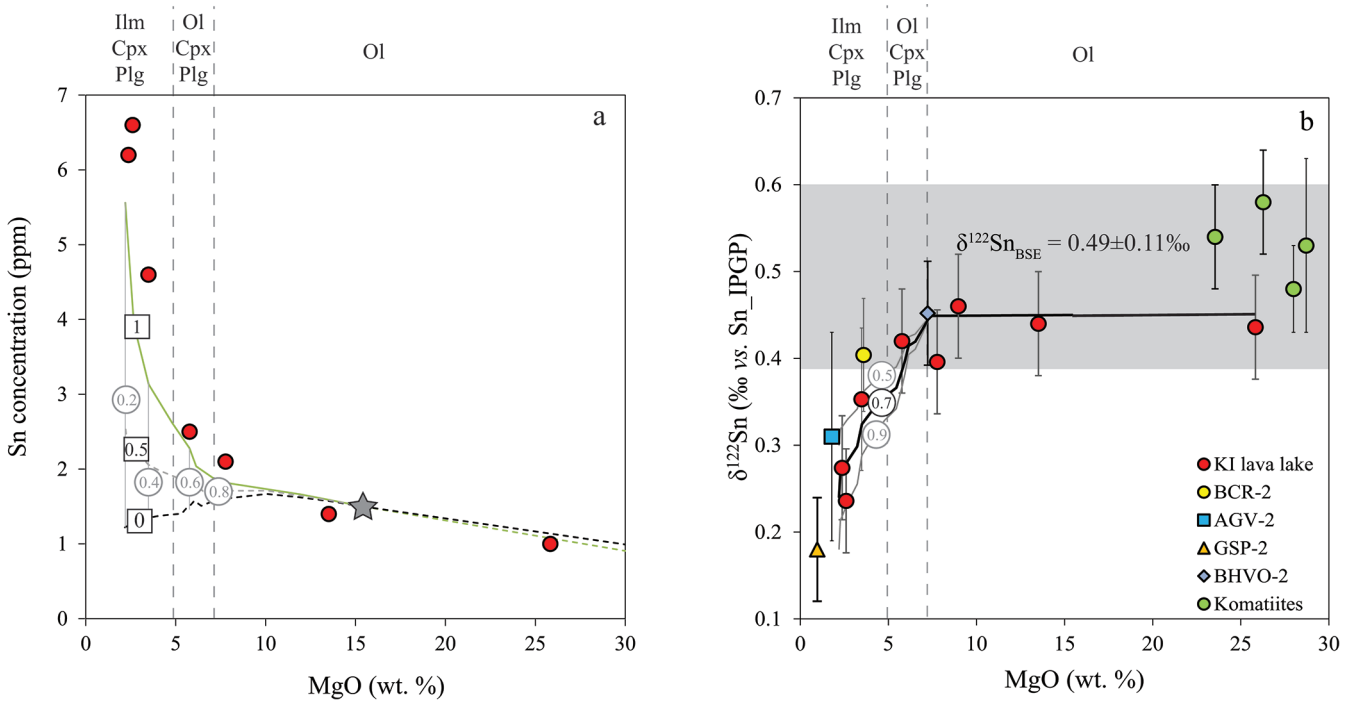

Figure 1 **(a)** Model showing Sn concentration for KI samples in the melt against MgO content. Red circles = KI samples. Thick lines represent modelled evolution with differing $Sn^{4+}/\sum Sn$, listed in black boxes from 1 (green line), 0.5 (dashed grey line) and 0 (dashed black line). Thin grey line represents the fraction of melt remaining (F), listed in grey circles, with the grey star representing the parental melt composition. **(b)** δ^{122}Sn and Sn against MgO (wt. %) for the KI lava lake samples. The solid lines represent the modelled δ^{122}Sn for $\Delta^{122}Sn_{mineral\text{-}melt}$ = 0.5 (grey line), 0.7 (black line) and 0.9 (grey line). Geostandard values are taken from Creech *et al.* (2017). In both cases, the crystallising assemblage is listed at the top of the figure (Ol = olivine, Cpx = clinopyroxene, Plg = plagioclase, Ilm = ilmenite).

Table 1 Tin isotopic composition of the samples analysed in this study.

Sample ID	Rock type	Weight (g)	MgO (wt. %)	Sn conc. (µg/g)	δ^{122}Sn (‰)	2 s.d.[b]	n
KI67-3-6.8	picro-Basalt	0.3546	25.83[a]	1.0	0.44	0.07	1
KI79-3-150.4	Basalt	0.2506	13.51[a]	1.4	0.43	0.07	2
KI67-3-58.0	Basalt	0.2664	8.91[a]	1.4	0.46	0.07	2
KI75-1-121.5	Basalt	0.2483	7.77[a]	2.1	0.40	0.07	2
KI75-1-75.2	Basalt	0.2460	5.77[a]	2.5	0.42	0.07	2
KI79-1R1-170.9	Basaltic-andesite	0.2410	3.48[a]	4.6	0.35	0.08	2
KI67-2-85.7	Basaltic-andesite	0.2475	2.60[a]	6.6	0.24	0.07	2
KI81-2-88.6	Andesite	0.2512	2.37[a]	6.2	0.27	0.07	2
331/783	Komatiite (Barberton, 3.48 Ga)	1.5415	26.27[c]	0.36	0.58	0.07	2
331/948	Komatiite (Yilgarn, 2.7 Ga)	1.1810	23.54[c]	0.25	0.54	0.07	2
SD6/400	Komatiite (Yilgarn, 2.7 Ga)	1.2648	27.99[c]	0.25	0.48	0.07	2
422/96	Komatiite (Munro, 2.7 Ga)	1.1968	28.71[c]	0.15	0.53	0.10	2

[a] SiO_2/MgO values for Kilauea Iki lava lake taken from Helz *et al.* (1994). [b] Maximum of either 2 times the standard deviation on the sample measurement or BCR-2 external reproducibility. [c] MgO value for komatiites taken from Sossi *et al.* (2016).

Based on the relative compatibility of Sn^{2+}, Sn^{4+} would accumulate in the melt as fractional crystallisation progresses, such that $\frac{Sn^{4+}}{\Sigma Sn} \rightarrow 1$ as the fraction of melt remaining, $F \rightarrow 0$.

Sn speciation during fractional crystallisation. The relative proportions of MgO and $FeO^{(T)}$ in the KI samples were modelled assuming fractional crystallisation (Fig. 2). The mineral/melt partition coefficients calculated for Sn (Table 2) were used to model the evolution of Sn in the melt.

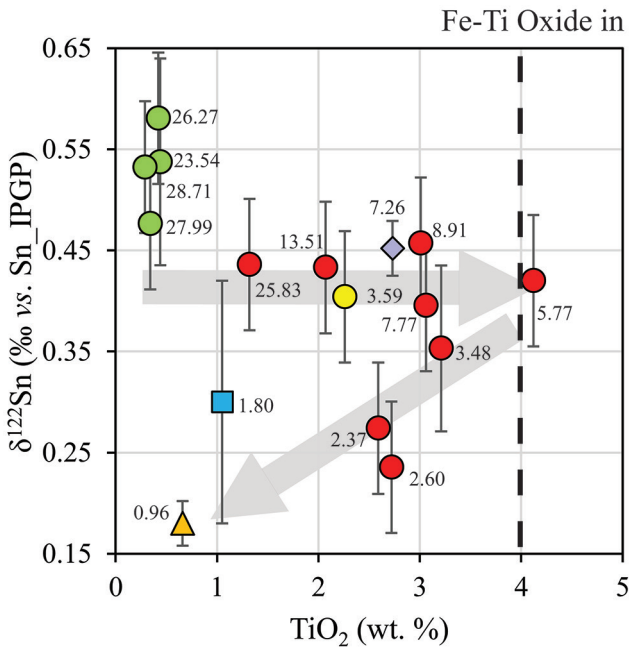

Figure 2 Variation of δ^{122}Sn with TiO_2 content, MgO (wt. %) shown next to the data point. Sn isotope fractionation occurs only after Fe-Ti oxide (ilmenite) saturation at Kilauea Iki. Symbols as per Figure 1.

The crystallising phase proportions of olivine, augite, plagioclase and Fe-Ti oxides were adjusted such that the modelled evolution of MgO and FeO contents closely follow the natural data, assuming $K_{D\ ol,aug-melt}^{Fe-Mg} = 0.3$ (Fig. 2). Olivine is the dominant crystallising phase until the MgO content falls to ~7.4 wt. % in the melt, as noted in Helz *et al.* (1994), at which point the liquid reaches the cpx + plg + ol cotectic, as shown by a change in slope of REE abundances against MgO (O'Neill, 2016; see Supplementary Information). Ilmenite then crystallises at the expense of olivine below ≈5 wt. % MgO (Fig. 2).

To evaluate the proportion of Sn^{2+} and Sn^{4+} in the melt, three distinct scenarios were considered: a) 100 % Sn^{2+}, b) $Sn^{2+}/Sn^{4+} = 1$ and c) 100 % Sn^{4+} (see Fig. 1a). The first two cases produce a) no increase in Sn concentration with MgO or b) a rise that is insufficient to describe the observed increase with MgO. Only scenario c), in which Sn is entirely stannic and thus strongly incompatible ($0.01 < \sum D^{min/melt} < 0.21$) reproduces the Sn evolution of the melt. Therefore, the Sn^{2+} species is likely very minor and the majority of Sn occurs as Sn^{4+}.

No experimental constraints exist for the equilibrium constant of Eq. 1 in basaltic liquids. However, a first order estimate of $\frac{Sn^{4+}}{\Sigma Sn}$ expected in magmatic systems comes from the experimentally derived relative reduction potential for the redox couple Sn^{4+} and Sn^{2+}; -4.4 V in $Na_2Si_2O_5$ melt (Schreiber, 1987). Using this value enables calculation of $Sn^{4+}/\sum Sn$ at the fO_2 (FMQ) and temperature (≈1200 °C) of the parental liquid, yielding a value of ≈0.9 (10 % Sn^{2+}). A caveat to this approach is that this result may not be applicable to basaltic melts. However, it also independently suggests that Sn^{4+} should predominate in terrestrial magmatic environments.

Isotopic behaviour of Sn during magmatic processes. Since Sn is likely tetravalent and coordinated by oxygen in the KI lava lake, the ~0.2 ‰ isotopic fractionation must reflect the difference in coordination number of Sn between the melt and the mineral assemblage. Sample KI79-3-150.4, with ~14 wt. % MgO (δ^{122}Sn = 0.46 ± 0.07 ‰), is close to the parental magma composition (Helz *et al.*, 1994). As olivine crystallises and accumulates at the bottom of the sequence, δ^{122}Sn is unchanged, because $D_{Fe,Zn}^{ol/melt} \approx 0$ (Fig. 1b). This behaviour contrasts with both Fe and Zn, whose isotopic fractionation is indeed controlled by olivine due to their relative compatibility in this phase, where $D_{Fe,Zn}^{ol/melt} = 1$, driving both δ^{57}Fe and δ^{66}Zn to heavier compositions to lower MgO (Teng *et al.*, 2008; Chen *et al.*, 2013). Only in samples with <5 wt. % MgO does δ^{122}Sn begin to decrease. Tin is weakly chalcophile, and its $D_{Sn}^{sulph/melt} = 5.3 \pm 3.6$ in KI samples (Greaney *et al.*, 2017). Sulphides are present in evolved basalts as isocubanite and bornite (having exsolved from high temperature intermediate solid solution), however their low modal abundance (<0.01 %; Stone and Fleet, 1991) means they have a negligible effect on the Sn budget of the magma. Furthermore, by analogy with Fe isotopes (Wawryk and Foden, 2017), Cu-bearing sulphides

Table 2 Calculated partition coefficients for Sn^{2+} and Sn^{4+} using lattice strain theory

	Coordination	Olivine	Orthopyroxene	Clinopyroxene	Plagioclase	Ilmenite
2+	*Lattice Strain*					
	VI	0.12 – 0.20	0.09 – 0.14	0.04 – 0.07	-	-
	VIII	-	-	1.0 – 1.2	0.94 – 1.27	-
	Bulk Sn^{2+}	0.12 – 0.20	0.09 – 0.14	1.04 – 1.27	0.94 – 1.27	-
4+	IV	$1x10^{-5}$	$1x10^{-5}$	$1x10^{-5}$	$1x10^{-5}$	-
	VI	0.005 – 0.01	0.01 – 0.07	0.05 – 0.39	-	4.5 – 6.8
	Bulk Sn^{4+}	0.005 – 0.01	0.01 – 0.07	0.05 – 0.39	-	-
Experimental						
Adam and Green (2006)		0.002 – 0.014	0.015	0.024 – 1	-	-
Klemme *et al.* (2006)		-	-	-	-	5.1
Michely *et al.* (2017)				0.19 – 0.46*		

*Only partition coefficients for the natural, komatiitic 'W' composition are reported here.

should harbour light Sn isotopes (contrary to observations), as also suggested by the long Sn-S bond length of 2.56 Å in SnS_2 (Hazen and Finger, 1979). Rather, comparison with TiO_2 shows that the decrease in $\delta^{122}Sn$ coincides with crystallisation of Fe-Ti oxides, predominantly ilmenite, in which Sn^{4+} is highly compatible (Klemme *et al.*, 2006; Table 2), further attesting to the predominance of Sn^{4+} in the melt. The TiO_2 content reaches a maximum of 4.12 wt. % at 5.77 wt. % MgO before dropping to 2.59 wt. % at 2.37 wt. % MgO (Fig. 2). Although the measured $D_{Sn}^{ilm/melt} = 0.63$ (Greaney *et al.*, 2017) is less than that determined experimentally (5.1), ilmenite nevertheless hosts 50 % of the Sn in solid phases. Coupled with its low modal abundance (≈5 %), $\sum D_{Sn}^{min/melt}$ remains below unity (0.2), and Sn continues to increase.

In order to replicate the change in Sn content and isotopic fractionation in the KI samples, a fractionation factor $\left(\Delta^{122}_{mineral-melt} Sn\right)$ of 0.7 ± 0.2 ‰ is required (see Supplementary Information), equivalent to 0.175 ± 0.050 ‰/amu. Sossi and O'Neill (2017) explored the effect of changing coordination environment on iron isotope fractionation, and found that the difference between IV-fold Fe^{2+} in chromite and VI-fold Fe^{2+} in ilmenite is only 0.05 ‰/amu at 1073 K, significantly smaller than that calculated for Sn. Nonetheless, the degree of enrichment of the light Sn isotopes in the more evolved samples is consistent with the observation of Creech *et al.* (2017) (Fig. 1b). This vector of fractionation to lighter Sn isotopes in the melt precludes the presence of Sn^{2+}, which, as it is concentrated in all crystallising phases relative to Sn^{4+}, and as a more reduced species, should result in heavy isotope enrichment in the melt. Rather, this argues for the lower coordination of Sn^{4+} in minerals relative to the melt. While the lattice strain model predicts that Sn^{4+} coordination (N) in minerals is 6-fold (Table 2), its coordination in the melt is poorly known. In melts with higher NBO/T (number of non-bridging oxygens per tetrahedral cation) than the hydrous granitic melts studied by Farges *et al.* (2006), Sn^{4+} may exist in 6 to 8-fold coordination by analogy with Sn^{2+}, which is in 8-fold coordination. While further XANES studies will help elucidate this issue, empirically, the shift to lighter Sn isotope compositions requires $\frac{C_N^{melt}}{C_N^{mineral}} > 1$.

The komatiites plot within uncertainty of the $\delta^{122}Sn$ plateau defined by KI lava lake samples with MgO > 5 wt. % (Fig. 1b). The komatiites analysed display spinifex textures, indicative of their formation from quenched liquids, representative of the parental magma. This consideration is not crucial for Sn, however, as olivine is the only mineral on the komatiite liquidus and its removal does not cause resolvable Sn isotope fractionation (Fig.1b), that is, $\delta^{122}Sn$ should remain constant irrespective of its position on an olivine control line.

Tin contents of the four komatiites positively correlate with La/Sm_N ratios (Fig. 3). The high degree of melting (25–40 %) undergone during komatiite formation results in quantitative extraction of incompatible elements, including Sn. Therefore, Sn depletion reflects that of its mantle source, where younger (2.7 Ga) komatiites experienced greater (up to 5 %) source depletion than the primitive mantle-derived 3.48 Ga komatiites (see Sossi *et al.*, 2016). Despite this variation in Sn contents (Fig. 3), the absence of isotopic fractionation between komatiite groups indicates that prior melt extraction (≤5 %) leaves the Sn isotopic composition of their mantle sources unchanged. Hawaiian basalts (0.44 ± 0.03, 2 s.d.) are isotopically indistinguishable (0.53 ± 0.08, 2 s.d.), and these asthenosphere-derived igneous rocks yield an average $\delta^{122}Sn$ = 0.49 ± 0.11 (2 s.d., n = 7). Owing to the constancy of Sn isotope composition in high MgO igneous rocks, and across several spatial and temporal domains, this value is taken to estimate the Sn isotope composition of the bulk silicate Earth.

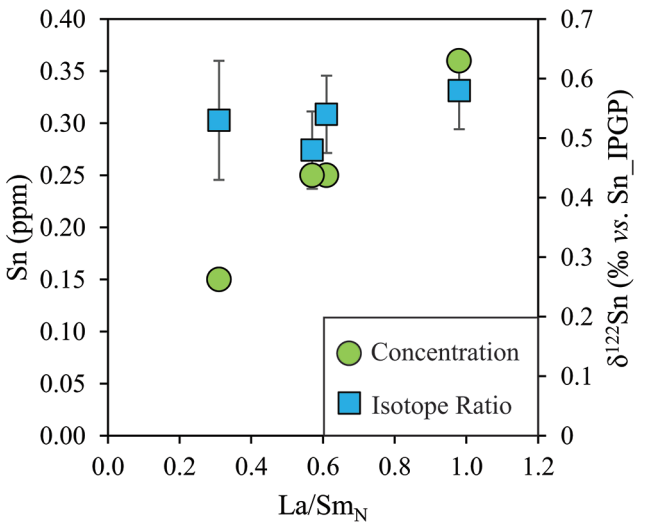

Figure 3 Depletion of komatiite source regions, quantified by La/Sm_N, as a function of Sn concentration (green circles) and $\delta^{122}Sn$ (blue squares). Tin contents are positively correlated with La/Sm_N, whereas $\delta^{122}Sn$ remains constant within uncertainty.

Acknowledgements

FM acknowledges funding from the European Research Council under the H2020 framework program/ERC grant agreement #637503 (Pristine) and support from the ANR through the Cradle project and the UnivEarthS Labex program at Sorbonne Paris Cité (ANR-10-LABX-0023 and ANR-11-IDEX-0005-02). Parts of this work were supported by IPGP multidisciplinary program PARI, and by Region Île-de-France SESAME Grant no. 12015908. We thank the two reviewers for constructive comments that have greatly improved the quality of the manuscript and Helen Williams for her careful and efficient edition of the paper.

Editor: Helen Williams

Additional Information

Supplementary Information accompanies this letter at www.geochemicalperspectivesletters.org/article1741

Cite this letter as: Badullovich, N., Moynier, F., Creech, J., Teng, F.-Z., Sossi, P.A. (2017) Tin isotopic fractionation during igneous differentiation and Earth's mantle composition. *Geochem. Persp. Let.* 5, 24–28.

References

Adam, J., Green, T. (2006) Trace element partitioning between mica-and amphibole-bearing garnet lherzolite and hydrous basanitic melt:1. Experimental results and the investigation of controls on partitioning behaviour. *Contributions to Mineralogy and Petrology* 152, 1–17.

Blundy, J., Wood, B. (1994) Prediction of crystal-melt partition coefficients from elastic moduli. *Nature* 372, 452–454.

Chen, H., Savage, P., Teng, F.Z., Helz, R., Moynier, F. (2013) Zinc isotope fractionation during magmatic differentiation and the isotopic composition of the bulk silicate Earth. *Earth and Planetary Science Letters* 369, 34–42.

Creech, J.B., Moynier, F., Badullovich, N. (2017) Tin stable isotope analysis of geological materials by double-spike MC-ICPMS. *Chemical Geology* 457, 61–67.

Farges, F., Linnen, R.L., Brown, G.E. (2006) Redox and speciation of tin in hydrous silicate glasses: A comparison with Nb, Ta, Mo and W. *Canadian Mineralogist* 44, 795–810.

Greaney, A.T., Rudnick, R.L., Helz, R.T., Gaschnig, R.M., Piccoli, P.M., Ash, R.D. (2017) The behavior of chalcophile elements during magmatic differentiation as observed in Kilauea Iki lava lake, Hawaii. *Geochimica et Cosmochimica Acta* 210, 71–96.

Hazen, R.M., Finger, L.W. (1979) Bulk modulus—volume relationship for cation-anion polyhedra. *Journal of Geophysical Research: Solid Earth* 84, 6723–6728.

Heinrich, C.A. (1990). The chemistry of hydrothermal tin (-tungsten) ore deposition. *Economic Geology* 85, 457–481.

Helz, R.T. (2012) Trace-element analyses of core samples from the 1967-1988 drillings of Kilauea Iki Lava Lake, Hawaii. *U.S. Geological Survey Report* 2010-1093.

Helz, R.T., Kirschenbaum, H., Marinenko, J.W., Qian, R. (1994) Whole-rock analyses of core samples from the 1967, 1979 and 1981 drillings of Kilauea Iki lava lake, Hawaii. *U.S. Geological Survey Report* 94-684.

Herzberg, C. (1992) Depth and degree of melting of komatiites. *Journal of Geophysical Research: Solid Earth* 97, 4521–4540.

Jenner, F., O'Neill, H. (2012) Analysis of 60 elements in 616 ocean floor basaltic glasses. *Geochemistry, Geophysics, Geosystems* 12, doi: 10.1029/2011GC004009.

Jochum, K.P., Hofmann, A.W., Seufert, H.M. (1993) Tin in mantle-derived rocks: Constraints on Earth evolution. *Geochimica et Cosmochimica Acta* 57, 3585–3595.

Kato, C., Moynier, F., Foriel, J., Teng, F.-Z., Puchtel, I.S. (2017) The gallium isotopic composition of the bulk silicate Earth. *Chemical Geology* 448, 164–172.

Klemme, S., Günther, D., Hametner, K., Prowatke, S., Zack, T. (2006) The partitioning of trace elements between ilmenite, ulvospinel, armalcolite and silicate melts with implications for the early differentiation of the moon. *Chemical Geology* 234, 251–263.

Maier, W.D., Barnes, S., Campbell, I., Fiorentini, M., Peltonen, P., Barnes, S., Smithies, H. (2008) Progressive mixing of meteoritic veneer into the early Earth's deep mantle. *Nature* 460, 620–623.

Médard, E., McCammon, C.A., Barr, J.A., Grove, T.L. (2008) Oxygen fugacity, temperature reproducibility, and H2O contents of nominally anhydrous piston-cylinder experiments using graphite capsules. *American Mineralogist* 93, 1838–1844.

Michely, L.T., Leitzke, F.P., Speelmanns, I.M., Fonseca, R.O.C. (2017) Competing effects of crystal chemistry and silicate melt composition on trace element behavior in magmatic systems: insights from crystal/silicate melt partitioning of the REE, HFSE, Sn, In, Ga, Ba, Pt and Rh. *Contributions to Mineralogy and Petrology* 172, 39.

O'Neill, H.S.C. (2016) The smoothness and shapes of chondrite-normalized rare Earth element patterns in basalts. *Journal of Petrology* 57, 1463–1508.

O'Neill, H.S.C., Palme, H. (2008) Collisional erosion and the non-chondritic composition of the terrestrial planets. *Philosophical transactions of the Royal Society A* 366, 4205–4238.

Paniello, R., Day, J.M.D., Moynier, F. (2012) Zinc isotopic evidence for the origin of the Moon. *Nature* 490, 376–379.

Schreiber, H.D. (1987) An Electrochemical Series of Redox Couples in Silicate Melts: a review and applications to geochemistry. *Journal of Geophysical Research* 92, 9225–9232.

Sossi, P.A., O'Neill, H.S.C. (2017) The effect of bonding environment on iron isotope fractionation between minerals at high temperature. *Geochimica et Cosmochimica Acta* 196, 121–143.

Sossi, P.A., Eggins, S.M., Nesbitt, R.W., Nebel, O., Hergt, J.M., Campbell, I.H., O'Neill, H., VanKranendonk, M., Davies, D. (2016) Petrogenesis and geochemistry of Archean komatiites. *Journal of Petrology* 57, 147–184.

Stone, W.E., Fleet, M.E. (1991) Nickel-copper sulfides from the 1959 eruption of Kilauea Volcano, Hawaii; contrasting compositions and phase relations in eruption pumice and Kilauea Iki lava lake. *American Mineralogist* 76, 1363–1372.

Teng, F.-Z., Dauphas, N., Helz, R.T. (2008) Iron Isotope Fractionation During Magmatic Differentiation in Kilauea Iki Lava Lake. *Science* 320, 1620–1622.

Tomascak, P.B., Tera, F., Helz, R.T., Walker, R.J. (1999) The absence of lithium isotope fractionation during basalt differentiation: new measurements by multicollector sector ICP-MS. *Geochimica et Cosmochimica Acta* 63, 907–910.

Wawryk, C.M., Foden, J.D. (2017). Iron-isotope systematics from the Batu Hijau Cu-Au deposit, Sumbawa, Indonesia. *Chemical Geology* 466, 159–172.

Witt-Eickschen, G., Palme, H., O'Neill, H., Allen, C. (2009) The geochemistry of the volatile trace elements As, Cd, Ga, In and Sn in the Earth's mantle: new evidence from in situ analyses of mantle xenoliths. *Geochimica et Cosmochimica Acta* 73, 1755–1778.

Geochemical Perspectives Letters

Tin isotopic fractionation during igneous differentiation and Earth's mantle composition

N. Badullovich[1], F. Moynier[1,2*], J. Creech[1], F.-Z. Teng[3], P.A. Sossi[1]

Supplementary Information

The Supplementary Information includes:

- Samples and Methods
- Tables S-1 and S-2
- Figures S-1 to S-4
- Supplementary Information References

Samples and Methods

Kilauea Iki lava lake

Located in the southeast of the Island of Hawai'i is the crystallised pit crater of Kilauea Iki. An eruption in 1959 saw lava pond into a pre-existing crater and fill to a depth of ~135 m (Richter *et al.*, 1970). As a result, lava cooled and crystallised resulting in a mostly closed system of fractional crystallisation. The interior was initially sampled in 1960–62 and the resulting cores are described in Richter and Moore (1966). Subsequent studies (Helz and Thornber, 1987; Helz *et al.*, 1994) have further documented the rocks in terms of geothermometry and trace element analysis. The parent magma is a picritic tholeiite with an average MgO content of 15.43 wt. % (Wright, 1973) and large-scale differentiation ceased around 1980 making the cooling period less than 30 years (Helz and Thornber, 1987). The surrounding country rock has a similar composition to the lava lake meaning country rock assimilation has a negligible effect on chemical composition. A study by Tomascak *et al.* (1999) identified that the time for the differentiation sequence to form, and subsequently be cored and collected, was significantly short on geological timescales. This means there has been insufficient time for fluid-rock interaction to occur. The samples utilised in this study from Kilauea Iki consist of eight rocks from the differentiation sequence with a marked systematic decrease in MgO content. The differentiation sequence samples form a sub-alkali series with MgO content ranging from 25.83 wt. % to 2.37 wt. % (Helz *et al.*, 1994). Rare Earth Elements are particularly diagnostic tracers of igneous processes because, as a group, their behaviour varies as a smooth function of ionic radius where their charge (3+) is constant across the lanthanide period. The properties of smooth, REE patterns may be quantified by fitting a polynomial to them. In order to identify which aspect of the pattern affects the polynomial fit, the polynomial can be written in an orthogonal form. That is, its coefficients are independent of each another, taking the form: $\ln([REE])/([REE]_N) = \lambda_0 + \lambda_1 x_1 + \lambda_2 x_2 + \lambda_3 x3 \ldots \lambda_n x_n$, where [*REE*] refers to the concentration of the REE pattern, normalised by CI chondrites, *N*. The *x* terms are defined such that the coefficients, λ, are independent of each other and the number of terms, *n*, in the equation. The λ coefficients describe the shape of the pattern, with each of them defining a specific property. The simplest, λ_0, is the average abundance of REE, λ_1 the average linear slope, and λ_2 the quadratic curvature (see O'Neill, 2016). A fundamental change in the fractionating mineral assemblage is observed at 7.4 wt. % MgO, where the mean Rare Earth Element abundance increase (quantified by λ_0) with MgO changes slope. This corresponds to the transition from olivine-dominated to crystallisation cpx + plg + ol cotectic, occurring at 1170 °C (Helz, 1987).

Analytical method

All samples were already in powdered form and around 0.250 g were measured out, depending on the Sn concentration in order to have ~0.5 µg total of Sn for each sample. The powders were transferred to Teflon beakers where concentrated HNO_3-HF (3:1) was added to facilitate the digestion process. All samples spent two days on the hotplate at 140 °C with 15 minutes in an ultrasonic bath after each day to break down any conglomerated sample. After total digestion was achieved the samples were dried down on the hotplate and then taken up in aqua regia (3:1 of concentrated HCl-HNO_3) to ensure all samples were in solution and to break down fluoride complexes. This stage was accompanied by the addition of the ^{117}Sn-^{122}Sn double spike to all samples. The double spike amounts varied depending on sample weight and Sn concentration (which was estimated to be 2 µg/g in all Kilauea Iki samples in order to spike). The samples were returned to the hotplate for another day to allow equilibration of the double spike with the sample. The samples were then dried down once again and taken up in concentrated HCl for conversion and then dried down again and taken up in 0.5 N HCl for column chemistry.

1. Institut de Physique du Globe de Paris, Université Sorbonne Paris Cité, Université Paris Diderot, 1 rue Jussieu, 75238 Paris cedex 05, France
2. Institut Universitaire de France, 75005 Paris, France
* Corresponding author (email: moynier@ipgp.fr)
3. Department of Earth and Space Sciences, University of Washington, Seattle, USA

To achieve Sn purification, the method outlined in Creech *et al.* (2017) was applied to all samples. Columns were loaded with 2 mL of TRU spec anion exchange resin and after cleaning were equilibrated with 10 mL of 0.5 N HCl. After matrix elements were eluted using 0.5 N and 0.25 N HCl, the Sn remaining was liberated from the column and collected using 0.5 N HNO_3. Measurement of the procedural blanks yielded Sn concentrations of <1 ng which is insignificant considering the amount of Sn in the samples (~0.5 µg). The final Sn cuts were dried down and taken up in 0.5 N HCl and diluted to achieve Sn concentration of 100 ppb for analysis on the Thermo Scientific Neptune Plus high resolution MC-ICP-MS at the Institut de Physique du Globe de Paris (procedures following Creech *et al.*, 2017). To visualise the Sn isotopic data from this study, delta notation is used relative to an in house standard produced at the Institut de Physique du Globe de Paris, Sn_IPGP (Creech *et al.*, 2017):

$$\delta^{122}Sn(‰) = \left(\frac{\frac{122}{118}Sn_{sample}}{\frac{122}{118}Sn_{Sn_{IPGP}}} - 1 \right) \times 1000 \qquad \text{Eq. S-1}$$

Measurements of samples were bracketed with measurements of the Sn_IPGP standard during the course of the different analytical sessions. All the samples were run during the same session as the results reported in Creech *et al.* (2017) with the exception of the komatiite samples that were run in a different session. Uncertainty was taken from the external reproducibility of the USGS standard BCR-2 (±0.065 ‰; see Creech *et al.* 2017), or as the 2 s.d. of the two measurements performed on each sample, whichever was larger.

Lattice strain theory

The lattice strain theory outlined in Blundy and Wood (1994) reports that the partitioning behaviour of any series of isovalent cations can be understood with a model where the main controls are the size and elasticity of the crystal lattice site. The calculated partition coefficient of an element (D_i) can be related to the partition coefficient of an ideal element (D_0) (for a particular site), the ideal radius (r_0) and Young's modulus (E) (Eq. S-2):

$$D_i(P,T,X) = D_0(P,T,X) \times \exp\left[\frac{-4\pi E N_A \left[\frac{r_0}{2}(r_i - r_0)^2 + \frac{1}{3}(r_i - r_0)^3 \right]}{RT} \right] \qquad \text{Eq. S-2}$$

The calculated partition coefficient will be a function of pressure, temperature and composition and the Young's modulus can be calculated for a different valence cations using the Hazen and Finger (1979) relationship. The values of D_0, E and r_0 used for the Sn partitioning calculations are outlined in Table S-1. The Sn^{2+} species can be hosted in the M1 sites of olivine, orthopyroxene and clinopyroxene in VI-fold coordination (based on charge and ionic radius constraints). Similarly, it can also be present in the M2 site of clinopyroxene and plagioclase in VIII-fold coordination. Its substitution is a simple one for other M^{2+} cations, and is thus energetically favourable.

The Sn^{4+} species in olivine, orthopyroxene and clinopyroxene partitions into the M1 site in VI-fold coordination and the T site in IV-fold coordination. Finally, ilmenite can only host Sn^{4+} in its M site in VI-fold coordination. In all cases, Sn^{4+} (r = 0.69 Å) behaves in a similar manner to Ti^{4+} (r = 0.605 Å), as shown for example, by the remarkable correlation between D_{Ti} and D_{Sn} in natural olivines (Witt-Eickschen *et al.*, 2009). In olivine, Ti is dominantly incorporated as the Ti-clinohumite end member, $MgTiO_2(OH)_2$, as point defects (Berry *et al.*, 2007), suggesting that Sn^{4+} contents in olivine may also be controlled by this mechanism. As Sn^{4+} is highly incompatible in olivine the mechanism is difficult to assess. In quadrilateral pyroxenes, however, Ti^{4+} is strongly ordered into the M1 site (*e.g.*, Adam and Green, 1994). Tetravalent titanium may be incorporated *via* two prevailing reactions (Morimoto, 1988), or a combination thereof:

$$(E^{2+})_{M2}(E^{2+})_{M1}2(E^{4+})_T O_6 \text{ É } (E^{+})_{M2}(E^{2+}_{0.5}\, Ti^{4+}_{0.5})_{M1}2(E^{4+})_T O_6 \qquad \text{Eq. S-3}$$

and

$$(E^{2+})_{M2}(E^{2+})_{M1}2(E^{4+})_T O_6 \text{ É } (E^{2+})_{M2}(E^{2+}_{0.5}\, Ti^{4+}_{0.5})_{M1}(E^{3+}E^{4+})_T O_6 \qquad \text{Eq. S-4}$$

which are in both cases, the coupled substitutions $3E^{2+}(2E^{+}Ti^{4+})^{-1}$, abbreviated NAT, and $2E^{4+}E^{2+}(2E^{3+}Ti^{4+})^{-1}$, abbreviated TAL, respectively. In natural pyroxenes, $E^{+} = Na^{+}$, $E^{2+} = Fe^{2+}$ or Mg^{2+}, and $E^{3+} = Al^{3+}$, where an assessment of terrestrial pyroxenes (Cameron and Papike, 1981) reveals that the TAL substitution is the most important mechanism for Ti substitution in all tectonic settings, particularly in Hawaiian basalts. It is therefore likely that Sn^{4+} is partitioned into pyroxenes *via* an analogous reaction to Eq. S-4. Indeed, the data of Michely *et al.* (2017) show that $D_{Sn}^{cpx/melt}$ increases systematically with the $^{IV}Al^{3+}$ in clinopyroxene, indicative of the TAL substitution. In their experiments, D_0 for 4+ cations on the M1 site increases with melt Na_2O content ($0.5 < D_0 < 2.3$) and E is higher (≈3,100 GPa) than derived from the Hazen-Finger relationship (575 GPa). Nonetheless, the measured $D_{Sn}^{cpx/melt}$ in natural komatiitic melt compositions (0.19 to 0.67) from Michely *et al.* (2017) overlaps with our calculated values (0.05 to 0.39) and is thus deemed fit for purpose considering differences in melt composition. In ilmenite, Sn^{4+} partitions by the simple direct substitution for octahedrally coordinated Ti^{4+}, yielding high $D_{Sn}^{ilm/melt} \approx 5$ (Klemme *et al.*, 2006). Table S-1 summarises the values used for the ideal parameters and bulk mineral properties when calculating Sn partition coefficients utilising the lattice strain theory outlined in Blundy and Wood (1994).

Deriving the VIII-fold radius of Sn^{2+}

There is no data available for this parameter and so we estimated the Sn^{2+} radius for VIII-fold coordination using the radius of Cd (1.11 Å). Tin is larger than Cd and so the estimate for its ionic radius is slightly higher at 1.15 Å. The difference between the VI-fold and VIII-fold coordination between other 2+ cations is between about 0.15 and 0.2 Å. We adopted this reasoning and assumed the difference between the VI-fold and VIII-fold coordinated Sn^{2+} to be 0.19 Å.

Major element modelling using fractional crystallisation equation

The Mg and Fe contents in the Kilauea Iki lava lake were modelled using the fractional crystallisation equation outlined in Shaw (1970). The purpose of the model was to replicate the trends of MgO and FeO described in Helz (1987) so that the phase proportions (olivine, clinopyroxene, plagioclase and Fe-Ti oxide) could be deduced and ultimately also the Sn concentration and Sn isotopic values (see below). Assuming perfect Rayleigh distillation and considering a perfectly incompatible element (*e.g.*, Th) then the fractional crystallisation equation simplifies to:

$$C_l = \frac{C_0}{F} \qquad \text{Eq. S-5}$$

Table S-1 Terms used for Sn partition coefficient calculations.

Phase Coordination		Olivine M1 (VI-fold)	Orthopyroxene M1 (VI-fold)	Clinopyroxene		Plagioclase M2 (VIII-fold)	Ilmenite M (VI-fold
				M1 (VI-fold)	M2 (VIII-fold)		
2+	r_i^{2+}	0.96 Å	0.96 Å	0.96 Å	1.15 Å	1.15 Å	-
	r_o^{2+}	0.72 Å (Mg^{2+})	0.72 Å (Mg^{2+})	0.72 Å (Mg^{2+})	1.06 Å (Ca^{2+})	1.06 Å (Ca^{2+})	-
	D_o^{2+}	4.2 - 7.0	3.1	1.5 - 2.5	1.0 - 1.35	1.0 - 1.35	-
	$\bar{E}^{2+}$	243 (GPa)	243 (GPa)	243 (GPa)	116 (GPa)	116 (GPa)	-
4+	r_i^{4+}	0.69 Å	0.69 Å	0.69 Å	-	-	0.69 Å
	r_o^{4+}	0.605 Å (Ti^{4+})	0.605 Å (Ti^{4+})	0.605 Å (Ti^{4+})	-	-	0.605 Å (Ti^{4+})
	D_o^{4+}	0.01 - 0.1	0.1	0.1 - 0.87	-	-	10 - 15
	$\bar{E}^{4+}$	575 (GPa)	575 (GPa)	575 (GPa)	-	-	575 (GPa)

Temperature (T) was taken as 1573 K, in the range of a typical basaltic melt.

where C_0 represents the bulk concentration of the element in question and F denotes the melt fraction. Using a perfectly incompatible element makes it possible to determine the F values in natural rocks, which then enables the evolution of MgO and FeO to be quantified. The modelling was performed for an F value between 1 and 0.2 at intervals of 0.05. The partition coefficients (for the major minerals) for Sn are taken from the lattice strain calculations.

The model requires starting compositions of FeO, MgO and Sn along with the partition coefficients of Sn between the major minerals. The starting composition of the melt is approximately equal to the sample KI79-3-150.4 which has an MgO content of ~13.5 wt. %. However, Wright (1973) determined the parental magma MgO content to be around 15.5 wt. % but this involved assumptions and a weighted average of different samples, in either case this will have little effect on the Sn content of the parental melt, which does not change markedly over this MgO interval. The model had a starting composition of 15.43 wt. % MgO, 11.2 wt. % FeO (Helz, 1987) and 1.5 µg/g Sn (taken from sample KI79-3-150.4). Figure S-1 shows the modelled Sn concentration evolution for all Sn^{4+}, all Sn^{2+} and when Sn^{2+}/Sn^{4+} = 1. It is clear that the model containing all Sn^{4+} best represents the Sn concentration data. For olivine accumulation, the models of Sn^{2+} and Sn^{4+} are too close to each other to be statistically significant and hence permit the possibility of Sn^{2+} being present in the parental magma and then partitioning into olivine.

Sn isotopic modelling of Kilauea Iki lava lake

The Sn isotopic fractionation in the lava lake is the result of fractional crystallisation and so the modelling is governed by the same Rayleigh equation:

$$R = R_0 F^{\alpha-1} \qquad \text{Eq. S-6}$$

where the fractionation factor in this case is given as the fractionation factor between the sum of the minerals and the melt. The fraction of Sn in the melt only begins to decrease significantly when clinopyroxene and ilmenite begin to crystallise and in order to achieve the observed Sn isotopic trends, an isotopic fractionation factor $\left(\Delta^{122}_{mineral-melt}Sn\right)$ of 0.7 ‰ is required along with a starting δ^{122}Sn value of 0.45 ‰. So, in order to calculate the δ^{122}Sn in the melt, the following equation was used along with the mineral-melt fractionation factor:

$$\delta^{122}Sn_{melt} = \delta_{122}Sn_{initial} + \Delta^{122}_{mineral-melt}Sn \times \ln\left(f_{Sn}\right) \qquad \text{Eq. S-7}$$

where f_{Sn} is the fraction of Sn remaining in the melt. The significant fractionation occurs in the MgO-poorest samples where the heavy Sn isotopes become compatible in ilmenite.

The two MgO-poorest samples record the lowest δ^{122}Sn values and this is the point of crystallising of Fe-Ti oxides (including ilmenite), at melt fraction of ~0.3. Table S-1 shows that Sn^{4+} is highly compatible in ilmenite ($D_{Sn} \approx 5$, substituting for Ti^{4+}) which agrees with experimental studies from Klemme *et al.* (2006). The Ti-O (octahedrally coordinated) bond length in ilmenite is 1.98 Å (Wechsler and Prewitt, 1984) whereas the Sn-O (octahedrally coordinated) bond length in a hydrous granitic melt was found by Farges *et al.* (2006) to be 2.03 Å. An Sn-O bond length of 1.98 Å in ilmenite would qualitatively describe its isotopic fractionation, as the δ^{122}Sn values continue decreasing for the two MgO-poorest samples, caused by partitioning of heavy Sn isotopes into ilmenite, resulting in an isotopically lighter melt (as observed in our data).

Table S-2 Average trace element ratio values for Kilauea Iki lava lake.

	Trace element ratio*	Value	Jochum *et al.* (1993) value	Jenner and O'Neill (2012)
Kilauea Iki	Sn/Hf	0.42 ± 0.08	0.41	0.45
	Sn/Zr	0.010 ± 0.0018	0.011	0.012
	Sn/Ta	1.3 ± 0.25	-	-
	Sn/Sm	0.26 ± 0.06	0.32	0.32

* Hf, Zr, Ta and Sm values taken from Helz and Taggart (2012).

Supplementary Figures

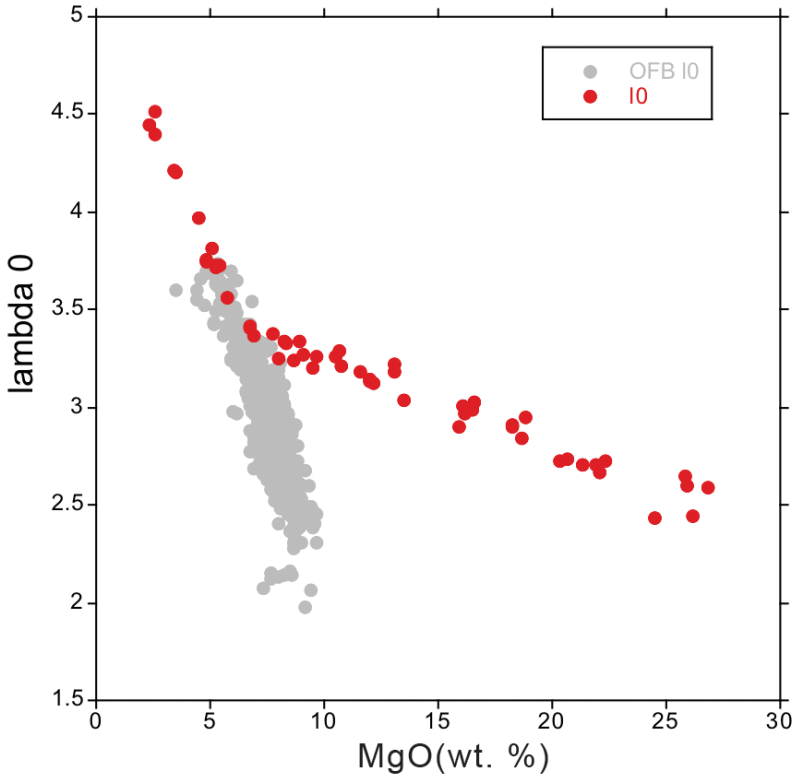

Figure S-1 Calculated λ_0, quantifying the mean abundances of the Rare Earth Elements (see O'Neill, 2016) against MgO. Red points correspond to the Kilauea Iki lava lake, and show a rapid drop in MgO and a small increase in λ_0 for 7.4 < MgO (wt. %) < 27 during olivine crystallisation/accumulation, before a rapid increase in slope at 7.4 wt. % MgO signalling a change in the crystallising assemblage to cpx + plg + ol.

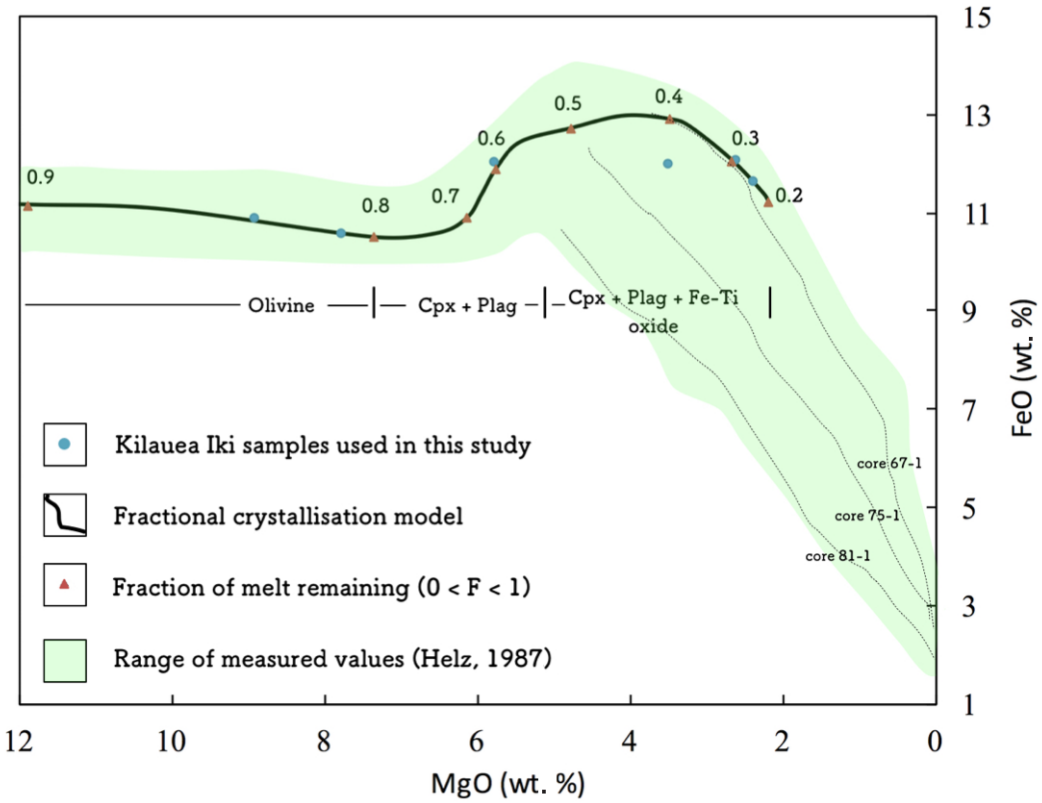

Figure S-2 Modelled abundances of FeO and MgO (wt. %) in the Kilauea Iki lava lake, overlain with the field (green) of literature data (Helz, 1987) for different eruption dates (1967, 1979 and 1981).

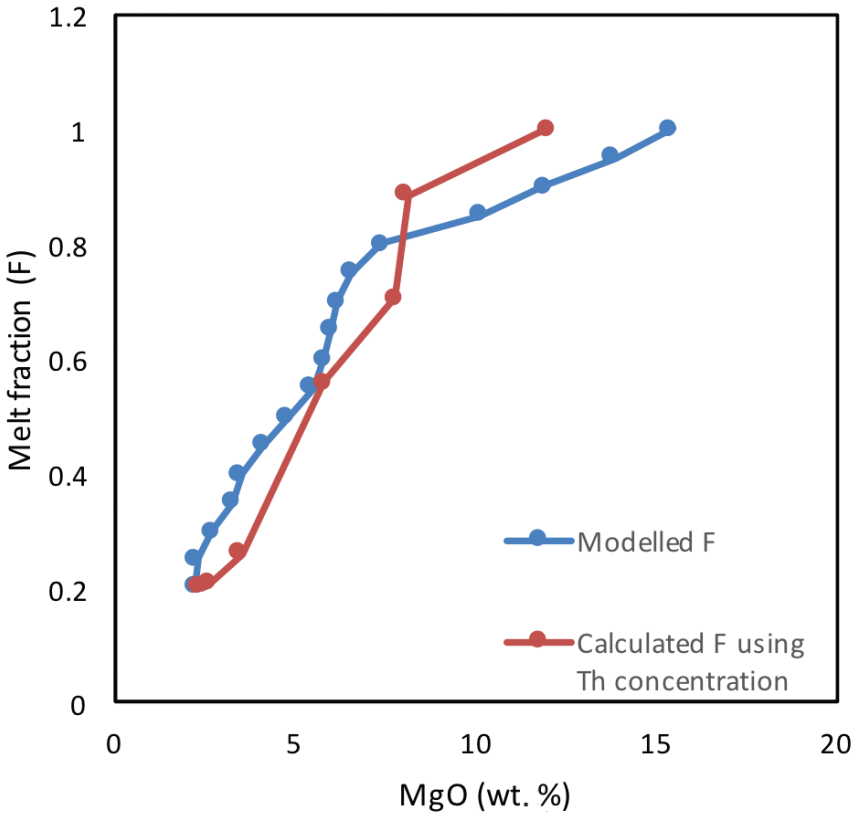

Figure S-3 Plot of melt fraction against MgO (wt. %). The maroon line represents the calculated F assuming that Th behaves as a perfectly incompatible element. The blue line represents the modelled F from the major element modelling of Kilauea Iki lava lake.

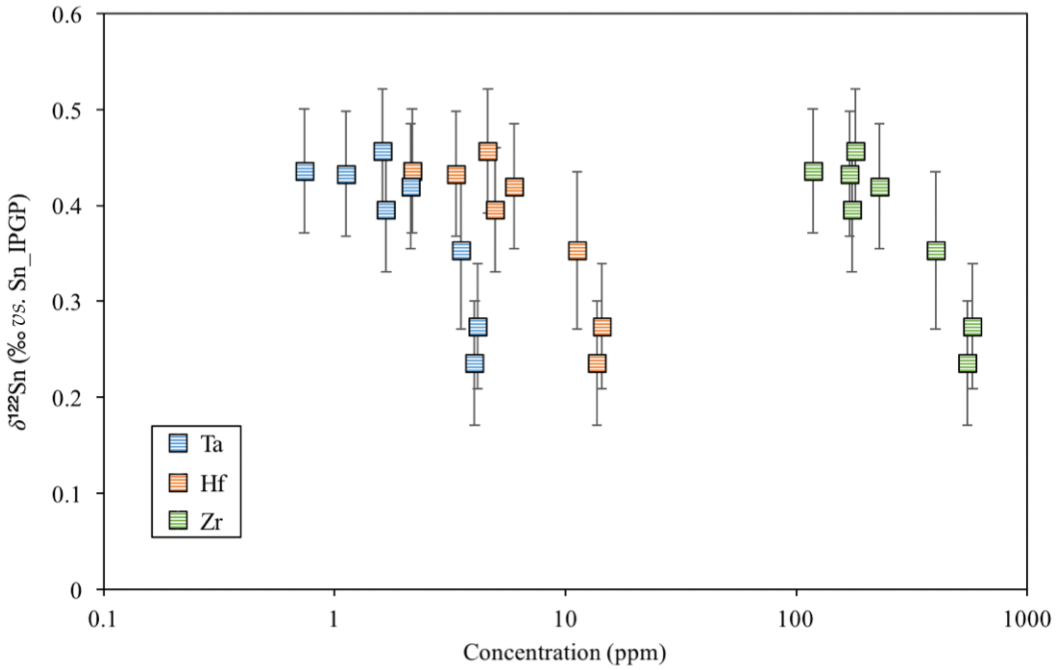

Figure S-4 Plot of δ^{122}Sn against Ta, Hf and Zr (HFSEs).

Supplementary Information References

ADAM, J., GREEN, T.H. (1994) The effects of pressure and temperature on the partitioning of Ti, Sr and REE between amphibole, clinopyroxene and basanitic melts. *Chemical Geology* 117, 219–233.

BERRY, A.J., O'NEILL, H.S.C., HERMANN, J., SCOTT, D.R. (2007) The infrared signature of water associated with trivalent cations in olivine. *Earth and Planetary Science Letters* 261, 134–142.

BLUNDY, J., WOOD, B. (1994) Prediction of crystal-melt partition coefficients from elastic moduli. *Nature* 372, 452–454.

CAMERON, M., PAPIKE, J.J. (1981) Structural and chemical variations in pyroxenes. *American Mineralogist* 66, 1–50.

CREECH, J.B., MOYNIER, F., BADULLOVICH, N. (2017) Tin stable isotope analysis of geological materials by double-spike MC-ICPMS. *Chemical Geology* 457, 61–67.

FARGES, F., LINNEN, R.L., BROWN, G.E. (2006) Redox and speciation of tin in hydrous silicate glasses: A comparison with Nb, Ta, Mo and W. *Canadian Mineralogist* 44, 795–810.

HAZEN, R.M., FINGER, L.W. (1979) Bulk modulus—volume relationship for cation-anion polyhedra. *Journal of Geophysical Research: Solid Earth* 84, 6723–6728.

HELZ, R.T. (1987) Differentiation behavior of Kilauea Iki lava lake, Kilauea volcano, Hawaii: an overview of past and current work. *Physicochemical principles* 1, 241–258.

HELZ, R.T., TAGGART JR., J.E. (2012) Trace-Element Analyses of Core Samples from the 1967–1988 Drillings of Kilauea Iki Lava Lake, Hawaii. *U.S. Geological Survey Open-File Report* 2010-1093.

HELZ, R.T., THORNBER, C.R. (1987) Geothermometry of Kilauea Iki lava lake, Hawaii. *Bulletin of Volcanology* 49, 651–668.

HELZ, R.T., KIRSCHENBAUM, H., MARINENKO, J.W., QIAN, R. (1994) Whole-rock analyses of core samples from the 1967, 1979 and 1981 drillings of Kilauea Iki lava lake, Hawaii. *U.S. Geological Survey Open-File Report* 94-684.

JENNER, F., O'NEILL, H. (2012) Analysis of 60 elements in 616 ocean floor basaltic glasses. *Geochemistry, Geophysics, Geosystems* 12, doi: 10.1029/2011GC004009.

JOCHUM, K.P., HOFMANN, A.W., SEUFERT, H.M. (1993) Tin in mantle-derived rocks: Constraints on Earth evolution. *Geochimica et Cosmochimica Acta* 57, 3585–3595.

KLEMME, S., GÜNTHER, D., HAMETNER, K., PROWATKE, S., ZACK, T. (2006) The partitioning of trace elements between ilmenite, ulvospinel, armalcolite and silicate melts with implications for the early differentiation of the moon. *Chemical Geology* 234, 251–263.

MICHELY, L.T., LEITZKE, F.P., SPEELMANNS, I.M., FONSECA, R.O.C. (2017) Competing effects of crystal chemistry and silicate melt composition on trace element behavior in magmatic systems: insights from crystal/silicate melt partitioning of the REE, HFSE, Sn, In, Ga, Ba, Pt and Rh. *Contributions to Mineralogy and Petrology* 172, 39.

MORIMOTO, N. (1988) Nomenclature of pyroxenes. *Mineralogy and Petrology* 39, 55–76.

O'NEILL, H.S.C. (2016) The smoothness and shapes of chondrite-normalized rare Earth element patterns in basalts. *Journal of Petrology* 57, 1463–1508.

RICHTER, D.H., MOORE, J.G. (1966) Petrology of the Kilauea Iki Lava Lake, Hawaii. *U.S. Geological Survey Professional Paper* 537-B.

RICHTER, D.H., EATON, J.P., MURATA, K.J., AULT, W.U., KRIVOY, H.L. (1970) Chronological narrative of the 1959-60 eruption of Kilauea Volcano, Hawaii. *U.S. Geological Survey Professional Paper* 537-E.

SHAW, D.M. (1970) Trace element fractionation during anatexis. *Geochimica et Cosmochimica Acta* 34, 237–243.

TOMASCAK, P.B., TERA, F., HELZ, R.T., WALKER, R.J. (1999) The absence of lithium isotope fractionation during basalt differentiation: new measurements by multicollector sector ICP-MS. *Geochimica et Cosmochimica Acta* 63, 907–910.

WECHSLER, B.A., PREWITT, C.T. (1984) Crystal structure of ilmenite (FeTiO3) at high temperature and at high pressure. *American Mineralogist* 69, 176–185.

WITT-EICKSCHEN, G., PALME, H., O'NEILL, H.S.C., ALLEN, C.M. (2009) The geochemistry of the volatile trace elements As, Cd, Ga, In and Sn in the Earth's mantle: new evidence from in situ analyses of mantle xenoliths. *Geochimica et Cosmochimica Acta* 73, 1755–1778.

WRIGHT, T.L. (1973) Magma Mixing as Illustrated by the 1959 Eruption , Kilauea Volcano, Hawaii Magma Mixing as Illustrated by the 1959 Eruption , Kilauea Volcano, Hawaii. *Geological Society of America Bulletin* 84, 849–858.